**PASJ:** Publ. Astron. Soc. Japan **48**, 237–248 (1996)

# X-Ray Properties of the Nucleus of M81

Yoshitaka ISHISAKI, Kazuo MAKISHIMA, and Naoko IYOMOTO
*Department of Physics, School of Science, The University of Tokyo, Hongo, Bunkyo-ku, Tokyo 113*
*E-mail (YI) ishisaki@miranda.phys.s.u-tokyo.ac.jp*

Kiyoshi HAYASHIDA
*Department of Earth and Space Science, Osaka University, Machikaneyama, Toyonaka, Osaka 560*

Hajime INOUE, Kazuhisa MITSUDA, Yasuo TANAKA, and Shin'ichiro UNO
*The Institute of Space and Astronautical Science, 3-3-1 Yoshinodai, Sagamihara, Kanagawa 229*

Yoshiki KOHMURA
*Institute for Physical and Chemical Research, 2-1 Hirosawa, Wako, Saitama 351-01*

Richard F. MUSHOTZKY, Robert PETRE, and Peter J. SERLEMITSOS
*Laboratory for High Energy Physics, NASA/GSFC, Greenbelt, MD 20771, USA*
and
Yuichi TERASHIMA
*Department of Astrophysics, Nagoya University, Chikusa-ku, Nagoya 464-01*

(Received 1995 September 25; accepted 1996 January 30)

**Abstract**

Due to the appearance of SN 1993J, the region of M81 (NGC 3031) was observed with ASCA ten times between 1993 April and 1995 April. Data from eight of these observations have been used to study the 0.5–10 keV spectral and temporal properties of the source designated X-5, coincident with the M81 nucleus. The 2–10 keV luminosity of X-5 varied by a factor of 1.7 over a period of two years, around a mean of $\sim 2 \times 10^{40}$ erg s$^{-1}$. Variations by $\sim 20\%$ on a time scale of one day were also detected. The average spectrum of X-5 can be represented in the 2–10 keV range by a power-law continuum of the photon index, $\Gamma = 1.85 \pm 0.04$, and a relatively low intrinsic absorption column of $N_{\rm H} \sim 1 \times 10^{21}$ cm$^{-2}$. In the soft ($< 2$ keV) energy range, an additional thermal component with a temperature of 0.6–0.8 keV has been detected. An apparently broad or complex Fe-K emission line centered at 6.6–6.7 keV was also detected at an equivalent width of $170 \pm 60$ eV. These results indicate that the M81 nucleus is a low-luminosity active galactic nucleus, and suggest that similar objects are relatively numerous. A comparison is made between the nucleus of M81 and those of Seyfert galaxies.

**Key words:** Galaxies: active — Galaxies: individual (M81) — Galaxies: X-rays

## 1. Introduction

M81 (NGC 3031) is a nearby (D $\sim$ 3.6 Mpc; Freedman et al. 1994) early-type spiral galaxy with a prominent bulge and well-defined spiral arms. Its nucleus shows weak Seyfert-like activity in the optical (Peimbert, Torres-Peimbert 1981; Shuder, Osterbrock 1982; Filippenko, Sargent 1988; Ho et al. 1995, 1996) and radio (Bartel et al. 1982; Beck et al. 1985) frequencies, and is considered to host a low-ionization nuclear emission-line region (LINER; e.g., Filippenko, Sargent 1985).

There are several different physical mechanisms that can give rise to the LINER phenomenon, including enhanced starburst activity (e.g., Terlevich, Melnick 1985) and the presence of an active galactic nucleus (AGN; which we identify with an accreting massive black hole) of low luminosity (e.g., Kwan, Krolik 1981). Although optical information is sometimes inadequate to distinguish between these two alternatives, in the X-ray band there is a clear spectral difference between them. Starburst galaxies have thermal X-ray spectra with emission lines from ionized metals (Makishima 1994, hereafter MA94; Tsuru et al. 1994; Serlemitsos et al. 1995b, hereafter SEA95), while AGNs exhibit power-law X-ray continua of photon index $\Gamma \sim 1.7$ (e.g., Turner, Pounds 1989) and often fluorescent Fe-K lines (e.g., Pounds et al. 1990; Awaki et al. 1991; Nandra 1991). X-ray variability (e.g., Krolik et al. 1993) provides more evidence for the presence of an AGN.

M81 has been observed in X-rays with Einstein ob-

Table 1. Log of ASCA observations of M81.

| ID | Date | | SIS | | | | GIS | |
|---|---|---|---|---|---|---|---|---|
| | Start* | End* | Exposure† | Mode‡ | X5 on§ | Split♯ | Exposure† | SP⋆ |
| 1 | 93/04/05 07:45 | 04/06 01:04 | — | 4CCD BRT | C0/C2 | 20 | (36039) | OF |
| 2 | 93/04/07 00:55 | 04/08 00:53 | — | 4CCD BRT | C0/C2 | 20 | (34421) | OF |
| 3 | 93/04/16 22:30 | 04/17 17:30 | 25537 | 4CCD F/B | C0/C2 | 40 | 99676 | OF |
| 4 | 93/04/25 14:10 | 04/25 21:31 | 10577 | 4CCD F/B | C0/C2 | 40 | 14214 | OF |
| 5 | 93/05/01 22:16 | 05/02 14:11 | 10550 | 4CCD F/B | C0/C2 | 40 | 27122 | OF |
| 6 | 93/05/18 20:47 | 05/19 20:30 | 23530 | 2CCD F/B | C0/C2 | 40 | 42864 | OF |
| 7 | 93/10/24 16:00 | 10/25 14:20 | 24250 | 4CCD F/B | C3/C1 | 40 | 43330 | ON |
| 8 | 94/04/01 05:08 | 04/02 03:21 | 28250 | 1CCD FNT | C0/C2 | 40 | 41515 | ON |
| 9 | 94/10/21 04:15 | 10/22 08:05 | 37423 | 1CCD FNT | C2/C0 | 40 | 51799 | ON |
| 10 | 95/04/01 18:50 | 04/02 23:10 | 14813 | 1CCD FNT | C0/C2 | 40 | 22625 | ON |

* The start time of observation in year/month/day hour:minutes, and the end time in month/day hour:minutes.

† Exposure time in seconds after the standard data screening described in text (subsection 3.1).

‡ The SIS mode. BRT= bright mode only, F/B = faint mode for high-bit-rate and bright mode for medium-bit rate, and FNT = faint mode only.

§ The chips of the SIS0/SIS1 detectors on which the M81 nucleus was placed.

♯ Pulse height channel for the SIS split threshold.

⋆ The GIS spread discriminator flag status.

servatory (Elvis, Van Speybroeck 1982; Fabbiano 1988, hereafter FA88), EXOSAT (Barr et al. 1985), Ginga (Ohashi et al. 1992; Tsuru 1992), BBXRT (Petre et al. 1993; hereafter PEA93), and ROSAT (Boller et al. 1992). The Einstein data (FA88) have revealed the presence of several X-ray sources in the M81 region, among which the brightest one, called X-5, coincides in position with the M81 nucleus and has an angular size $< 4''$ ($< 70$ pc; Elvis, Van Speybroeck 1982). In these previous observations, X-5 exhibited a 2–10 keV luminosity a few times $10^{40}$ erg s$^{-1}$, together with evidence of long-term variability and an episode of rapid flux change (Barr et al. 1985). These X-ray studies have led to the conclusion that X-5 is a low-luminosity AGN (LLAGN) in M81. However, discrepant spectra have been obtained for X-5 with Einstein ($\Gamma = 4^{+2}_{-1.5}$) and other observations ($\Gamma = 2.0$–$2.2$; Boller et al. 1992; Ohashi et al. 1992; Tsuru 1992; PEA93).

Due to the explosion of SN 1993J in M81 on 1993 March 28 (Garcia 1993), just 5 weeks after the launch of ASCA (Tanaka et al. 1994), we have frequently observed the M81 region with ASCA. The results concerning SN 1993J from these observations have been reported by Kohmura et al. (1994) and Kohmura (1994). These observations have also provided data of unprecedented quality and quantity on M81 X-5, which was always in the same ASCA field of view as SN 1993J. These results greatly strengthen the case that X-5 is an LLAGN. Some of these ASCA results concerning X-5 have already been reported by Ishisaki (1994) and SEA95.

## 2. Observations and Data Reduction

### 2.1. *Observations*

We observed the M81 region ten times with ASCA, as summarized in table 1. Six of these were performed between April 5 and May 19 in 1993 during the performance verification (PV) phase, almost once a week. The subsequent four observations were performed at intervals of six months, as dictated by sun-angle constraints of the satellite (Tanaka et al. 1994).

In these observations, data from the two GIS (Gas Imaging Spectrometer; Kohmura et al. 1993; Ohashi et al. 1996) detectors, GIS2 and GIS3, were always taken in the PH normal mode. For observations 1 through 6, the GIS spread discriminator was disabled, which caused a high background toward the detector rims, and a faint spill-over of counts from the $^{55}$Fe calibration isotope at certain positions on the detector plane (which does not affect the present results). The observation modes of the two SIS (Solid-State Imaging Spectrometer; Burke et al. 1991, 1994) detectors, SIS0 and SIS1, are listed in table 1. Each SIS detector comprises four CCD chips named C0 through C3.

### 2.2. *X-Ray Images*

In figure 1 we show examples of the SIS and GIS images of the M81 region. There were thus always three X-ray sources in the SIS field of view (figure 1a): X-5 at the M81 nucleus, the Einstein source X-6 (probably

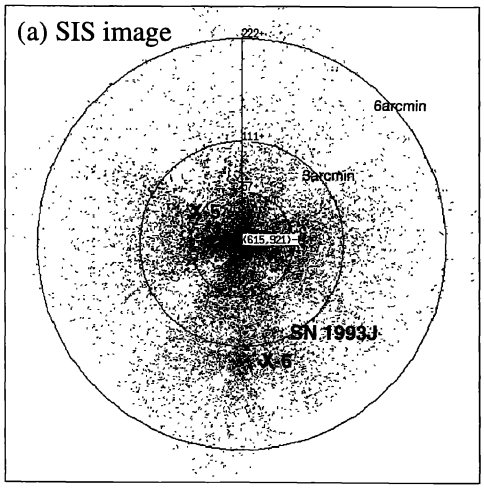


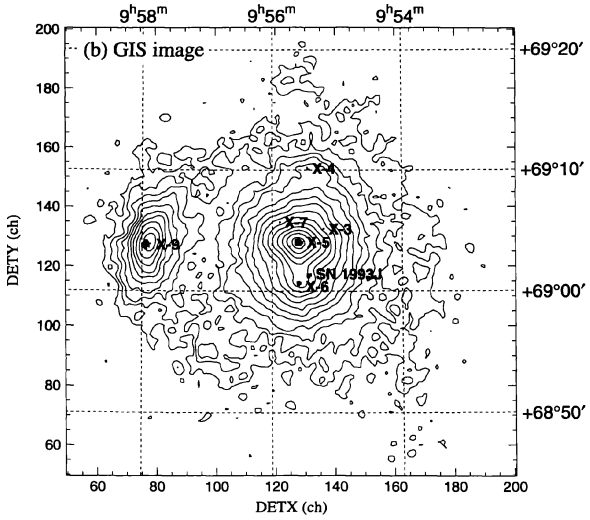


Fig. 1. X-ray images of the M81 region taken with ASCA, presented without background subtraction or vignetting correction. (a) The 0.5–10 keV SIS0 image from observation 7. SN 1993J and two Einstein sources, X-5 (the M81 nucleus) and X-6, are seen. Circles of radius 1.′5, 3′, and 6′ are drawn centered on X-5. (b) The 0.7–10 keV GIS2+GIS3 contour map smoothed with a Gaussian distribution of $\sigma$=15″, obtained by summing data for observations 7–9. The contour levels are 2.8, 4, 5.7, 8, ... c pixel$^{-1}$. An archival ROSAT HRI image taken on 1993 May, and the IPC source names, are overlaid. Sky coordinates are J2000, in which X-5 is located at ($9^h55^m33^s$, +69°03′55″).

a bright X-ray binary; FA88), and SN 1993J. The 0.5–10 keV raw intensities of X-5 and X-6 were in the ranges 0.32–0.56 and 0.05–0.07 c s$^{-1}$ per each SIS detector, respectively (Kohmura 1994). The 0.5–10 keV SIS intensity of SN 1993J was $\sim$ 0.08 c s$^{-1}$ (per SIS) in the first two observations, and then declined with a typical $e$-folding time of $\sim$ 70 d (Kohmura 1994). Thus, by the time when the ASCA images in figure 1 were obtained, SN 1993J had become much fainter ($\sim$ 0.02 c s$^{-1}$ or less) than during early observations (Kohmura et al. 1994).

In the GIS image (figure 1b), SN 1993J and X-6 are confused because their angular separation ($\sim$ 1′) is smaller than the GIS position resolution. In addition to X-5, X-6, and SN 1993J, we always detected another Einstein source, X-9, which is probably a background quasar (FA88). The GIS data for X-9 indicate a flat power-law ($\Gamma \sim 1.7$) spectrum and a moderate (factor $\sim$ 1.5) intensity variation. These results on X-9, as well as on X-6, will be reported in a forthcoming paper (Uno et al. 1994, in preparation), in which the latest results on SN 1993J will also be described.

### 2.3. *Data Reduction*

In the present paper, we utilize both the SIS and GIS data. For the SIS, we use only the faint mode data to avoid a subtle (typically by 10–30 eV) energy-scale ambiguity due to offset in the zero point (known as Dark Frame Error; Otani, Dotani 1994, private communication). We discard the SIS and GIS data from the first two observations, because, on these occasions, SN 1993J was too bright (subsection 2.2) to ignore its contamination of X-5, and the SIS data were taken entirely in the bright mode.

For the SIS event selection from the remaining eight observations, we required the geomagnetic cut-off rigidity to be $>$ 6 GeV c$^{-1}$, and the elevation angle from the night and day earth rim to be $>$ 10° and $>$ 25°, respectively. For the GIS event selection, we used the same cut-off rigidity and a minimum earth elevation angle $>$ 5°. These criteria have left us with 343 ks of good data for the GIS and 175 ks for the SIS.

The point-spread function of the ASCA X-ray telescope (XRT; Serlemitsos et al. 1995a; Tsusaka et al. 1995) caused significant contamination within the X-5 region from SN 1993J and X-6, which are 2.′8 and 3.′4 away from X-5, respectively. If we adopt 1.′5 (or 3.′0) as the integration radius around X-5, roughly 30% (or 70%) of the photons from SN 1993J and 30% (or 50%) of the photons from X-6 falls onto the X-5 accumulation region. Further taking into account the relative intensities among the three sources (subsection 2.2), we have set the integration radius around X-5 to be 1.′5 for observations 3 and 4 when SN 1993J was bright, and 3.′0 for the subsequent observations to collect as many signal pho-

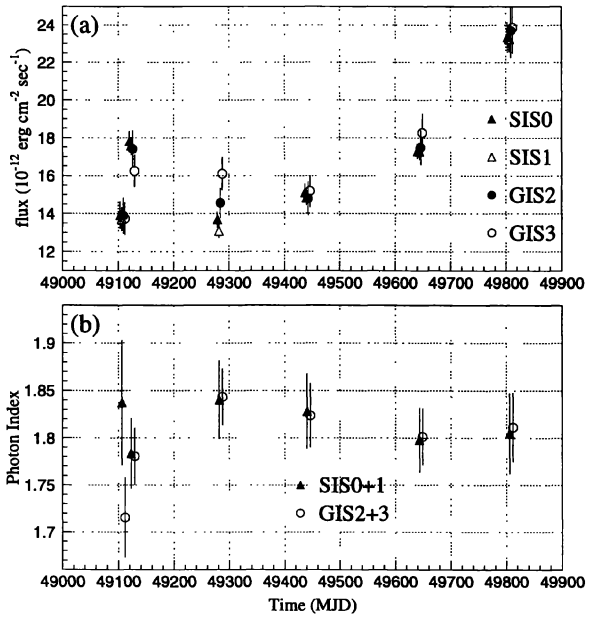


Fig. 2. Long-term 2–10 keV light curves of the M81 nucleus for observations 5 through 10, together with the 90% confidence errors. (a) The 2–10 keV flux history, obtained with SIS0+SIS1 and GIS2+GIS3. At the 3.6 Mpc distance, a flux $15 \times 10^{-12}$ erg cm$^{-2}$ s$^{-1}$ corresponds to a luminosity $2.2 \times 10^{40}$ erg s$^{-1}$. The observation number is given at the top. (b) History of the power-law photon index in the 2–10 keV range, determined independently with the two instruments.

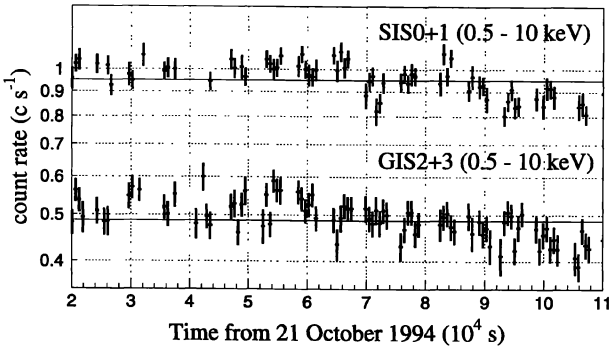


Fig. 3. Short-term 0.5–10 keV light curves of the M81 nucleus from observation 9. The upper light curve is the sum of SIS0 and SIS1, while the lower one is the sum of GIS2 and GIS3. Each bin is 600 s long, and errors are $1\sigma$. Solid lines indicate averaged counting rates (0.95 c s$^{-1}$ for the SIS and 0.49 c s$^{-1}$ for the GIS).

tons as possible. The contribution from SN 1993J plus X-6 to the events accumulated around X-5 is estimated to be 5–10% at most.

For the spectral analysis and flux calculations, we subtracted the background (the cosmic X-ray background plus non-X-ray background; Kubo et al. 1994, private communication; Ikebe et al. 1995, private communication; Makishima et al. 1996) accumulated over the same detector positions using blank-sky data (the M81 galaxy background is not subtracted, and estimated later in subsection 3.4.). For the SIS, the publicly released data (Gendreau 1994, private communication) were used. We made the GIS background from the Lynx field and the Lockman Hole data for observations 1–6 when the spread discriminator was still off, while we used the NEP, QSF3, Draco, and SA57 fields for observations 7–10 which occurred after the spread discriminator was enabled.

The XRT+SIS and XRT+GIS response files were calculated separately for the four detectors, and separately for each observation, because on different occasions the target was observed at different positions in the field of view. The responses take into account all of the known instrumental characteristics of the XRT (Kunieda et al. 1995, private communication; Tsusaka et al. 1995), the SIS (Burke et al. 1991, 1994), and the GIS (Ishida et al. 1994, private communication; Makishima et al. 1996).

## 3. Results

### 3.1. *Intensity and Spectrum Variability*

In figure 2a we present the background-subtracted long-term light curve of X-5 in the 2–10 keV band, for observations 5–10. The flux was calculated using the instrumental responses mentioned above. We omitted the results from observations 3 and 4, due to the relatively large flux uncertainties associated with the small integration radius required because of SN 1993J. Thus, the four detectors consistently indicate that the X-5 flux varied significantly over $(1.4\text{–}2.4) \times 10^{-11}$ erg cm$^{-2}$ s$^{-1}$, by a factor $\sim$ 1.7, implying a 2–10 keV luminosity range of $(2.1\text{–}3.5) \times 10^{40}$ erg s$^{-1}$ (employing the 3.6 Mpc distance). We estimated these absolute flux levels to be reliable within $\sim \pm 15\%$.

Figure 3 shows the short-term light curve of X-5 from observation 9. Both instruments thus suggest an overall $\sim$ 20% intensity decline, particularly toward the latter half of the observation, which is far too large to be caused by spacecraft attitude jittering. When the light curves were examined against the hypothesis of constant intensity, we obtained $\chi^2/\nu = 217/68$ with the SIS and 183/88 with the GIS, so that the hypothesis is rejected. We therefore conclude that a short-term intensity change was detected in this particular observation on a time scale

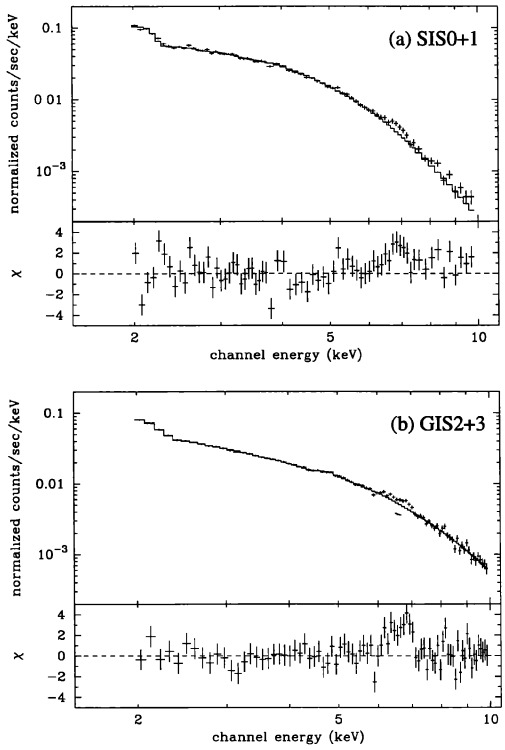


Fig. 4. SIS (panel a) and GIS (panel b) spectra of the M81 nucleus in the 2–10 keV band, both summed over observations 3–10. The solid lines show the best-fit power-law model convolved through respective instrumental responses, and the fit residuals are shown in lower panels. The fitting ignored the 6–7.5 keV region, where the iron line feature is clearly seen.

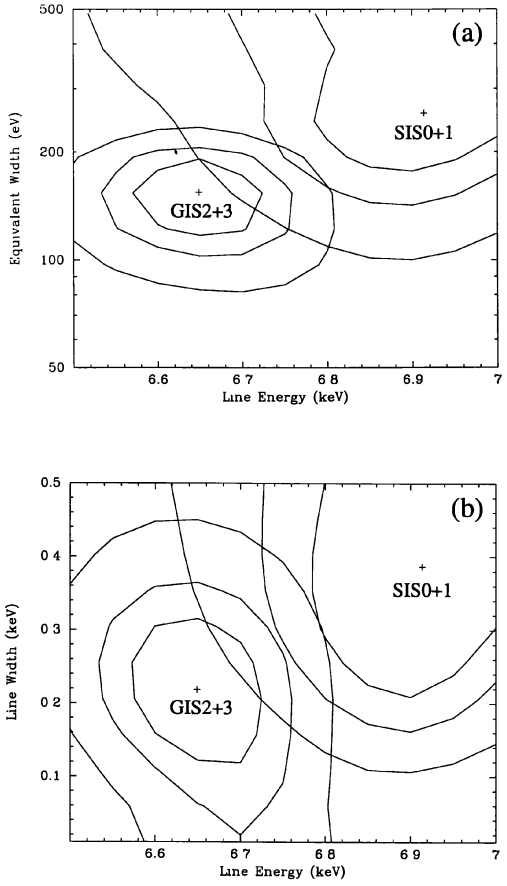


Fig. 5. Confidence contours of the iron line parameters, determined separately with the SIS and GIS by fitting a broad Gaussian model to the spectra of figure 4. Contours (from inner to outer) represent 68, 90, and 99% confidence levels, and the cross indicates the best-fit solution. (a) Line center energy vs. line equivalent width. (b) Line center energy vs. line width (Gaussian $\sigma$).

of about one day. A similar short-term variation was seen in observation 3, as reported by SEA95. There is no evidence for such a short-term variation in the other observations, with typical upper limits of $\sim$ 15%. We recall that a rapid ($\sim$ 600 s) variation was once recorded from M81 by EXOSAT (Barr et al. 1985), and possibly with the Einstein IPC (FA88).

The X-5 spectra are relatively featureless. In order to obtain a rough idea of the spectral variation, we fitted the 2–10 keV spectra from individual observations, separately for the two instruments, with a power-law model. We used the instrumental responses derived in subsection 2.3. The fit evaluation included 3% systematic errors. An acceptable fit was obtained in all cases. As shown in figure 2b, the spectral variability is statistically insignificant, in spite of the clear long-term intensity variation. We estimated the spectral index to have remained constant within $\pm$0.05, around a mean value of $\Gamma \sim 1.81$.

### 3.2. *Average 2–10 keV Spectra*

Since the spectral variations are insignificant, we summed up all of the SIS (SIS0+SIS1) data into a single spectrum, and all of the GIS (GIS2+GIS3) data into another, as shown in figure 4. Unlike in the previous subsection, we included the data from observations 3 and 4 as well. This allowed us to utilize one of the longest exposure times (343 ks for the GIS and 175 ks for the SIS) achieved with ASCA for a single object. We also calculated the average XRT+SIS and XRT+GIS responses, as averages of those for individual observations (sub-

Table 2. Model fits to the 2–10 keV spectrum of the M81 nucleus.

| | SIS | | GIS | |
|---|---|---|---|---|
| Model* | $\chi^2$/d.o.f. | Parameter† | $\chi^2$/d.o.f. | Parameter† |
| Bremsstrahlung | 252/70 | $kT$=8.8 keV | 290/82 | $kT$=8.6 keV |
| Power-law | 136/70 | $\Gamma$=1.79 (1.76–1.81) | 130/82 | $\Gamma$=1.83 (1.81–1.84) |
| Power-law+Gaussian distribution‡ | 103/67 | $\Gamma$=1.82 (1.79–1.85) | 78/79 | $\Gamma$=1.86 (1.84–1.88) |

* Absorption is fixed to the Galactic line-of-sight value ($N_{\rm H} = 4 \times 10^{20}$ cm$^{-2}$).
† $\Gamma$ is photon index, whose 90% confidence ranges are shown in parentheses.
‡ See figure 5 for the best fit values.

section 2.3) weighted by the number of detected signal photons. Using these responses, we fitted the summed SIS and GIS spectra separately in the 2–10 keV range with thermal bremsstrahlung and power-law models. As shown in table 2, the bremsstrahlung model could fit neither spectrum well ($\chi^2/\nu \sim 3.5$). This confirms the BBXRT result (PEA93), but with a much higher significance.

The power-law model with $\Gamma \sim 1.8$ was much more successful (table 2), indicating that the 2–10 keV continuum from X-5 definitely prefers a non-thermal interpretation to a thermal one. The obtained values of $\Gamma \sim 1.8$ are consistent with those derived from individual observations (figure 2b). However, these fits were still unacceptable, because of significant positive residuals in the 6–7 keV range in both spectra (figure 4). This feature was not significant in the individual spectra because of insufficient statistics. The feature is most naturally attributed to Fe-K emission lines, which have been observed mainly at 6.4 keV (corresponding to ionization states less than Fe XVII) from a number of AGNs (e.g., Pounds et al. 1990; Awaki et al. 1991; Nandra 1991). However, in the present case, the line appears to be broader than the instrumental energy resolutions ($\sim$ 0.1 and $\sim$ 0.45 keV for the SIS and the GIS respectively, in FWHM).

In order to model the line feature, we fitted the summed 2–10 keV spectra with a power-law model, plus a Gaussian distribution of which the center, width, and normalization were left free. The fit is improved, especially for the GIS spectrum (table 2), as far as the Gaussian distribution is allowed to be broad. Therefore, the presence of the line feature and its intrinsic width are both statistically significant. However, as shown in figure 5, the line parameters from the two instruments can be reconciled only at the 99% confidence level, and the SIS fit remains unacceptable (which makes the SIS contours in figure 5 rather meaningless). Since the SIS response exhibits more complex long-term changes (Otani, Dotani 1995, private communication) than the GIS, we suspect that our particular SIS spectrum, averaged over many observations spanning 2 years, may be subject to larger systematic errors. In fact, using a subset of the present ASCA data for X-5, SEA95 derived Fe-K line parameters from the two instruments that are both consistent with the present GIS results. We therefore refer mainly to the GIS-derived Fe parameters in the following, and defer any detailed comparison of the SIS and GIS Fe line parameters to a forthcoming paper (Yaqoob et al. 1996, in preparation).

Are the iron line photons really coming from the X-5 region? In fact, a broad Fe-K line centered at $\sim$ 6.8 keV was detected from SN 1993J (Kohmura et al. 1994; Kohmura 1994). However, the calculated contamination from SN 1993J can explain at most 15% of the line photons seen in the X-5 spectra. Furthermore, the iron-line source is mostly confined to within $\sim 3'$ ($\sim$ 3 kpc) of the M81 nucleus, since the line flux did not significantly increase when we increased the data-integration radius around X-5 up to $6'$. We thus conclude that almost all of the observed iron line photons come from the data-integration region around X-5.

In Seyfert galaxies, a spectral hump is produced in the 7–20 keV range by Compton-reflection effects (Pounds et al. 1990; Awaki et al. 1991). In a search of this effect in the X-5 data, we added a strongly absorbed power-law component to fit the average GIS spectrum. We tied its photon index to that of the main power-law, and fixed its absorption at $3 \times 10^{23}$ cm$^{-2}$ in order to approximate the reflection effect (Awaki et al. 1991). However, even when allowing the main power-law and Gaussian parameters to float, the reflection component was not required, with its normalization $<$ 12% (90% confidence) of the main power-law. This is significantly lower than is typically found ($\sim$ 30%) in Seyfert galaxies (Pounds et al. 1990).

### 3.3. *Spectra in the Full Energy Range*

In order to fully utilize the spectroscopic capabilities of ASCA, we expanded the range of the power-law plus Gaussian fit to 0.5–10 keV for the SIS, and 0.7–10 keV

Table 3. Model fits to the spectrum of the M81 nucleus in the full energy range.*

| | SIS (in 0.5–10 keV) | GIS (in 0.7–10 keV) |
|---|---|---|
| Model 1 : Absorbed power-law + Gaussian distribution† | | |
| Photon Index | 1.87 (1.85–1.89) | 1.82 (1.81–1.84) |
| $N_{\rm H}$ ($10^{20}$ cm$^{-2}$) § | 9.2 (8.5–9.8) | 4.7 (3.4–6.0) |
| $\chi^2$/d.o.f | 133/95 | 122/96 |
| Model 2: Raymond-Smith‡ + Absorbed power-law + Gaussian distribution† | | |
| $kT$ (keV) | 0.86 (0.70–1.10) | 0.71 (0.63–0.80) |
| $L_{0.5-3}^{\rm R-S}$ ($10^{38}$ erg s$^{-1}$) ♯ | 3.1 (1.2–6.3) | 19 (13–28) |
| Photon index | 1.85 (1.83–1.87) | 1.87 (1.85–1.90) |
| $N_{\rm H}$ ($10^{20}$ cm$^{-2}$) § | 9.4 (8.8–10.1) | 17.3 (12.9–22.4) |
| $L_{2-10}^{\rm P-L}$ ($10^{40}$ erg s$^{-1}$) ♯ | 2.40 (2.37–2.43) | 2.32 (2.30–2.34) |
| $\chi^2$/d.o.f | 123/93 | 96/94 |

* The numbers in parenthesis represent the 90% confidence range.
† The Gaussian parameters are fixed to the values from the 2–10 keV fit.
‡ Assumed to have an abundance of 0.4 times solar, and absorbed by the line-of-sight galactic column of $N_{\rm H} = 4 \times 10^{20}$ cm$^{-2}$.
§ Absorption includes the line-of-sight galactic column of $N_{\rm H} = 4 \times 10^{20}$ cm$^{-2}$.
♯ $L_{0.5-3}^{\rm R-S}$ is the 0.5–3 keV luminosity of the Raymond-Smith component, while $L_{2-10}^{\rm P-L}$ is the 2–10 keV luminosity of the (unabsorbed) power-law component.

for the GIS. We allowed both $\Gamma$ and the column density $N_{\rm H}$ to float. For fitting the SIS (or GIS) spectrum, we fixed the Gaussian parameters at those obtained above 2 keV with the SIS (or GIS). The results of these fits are summarized in table 3. Although the value of $\Gamma$ is similar to those obtained in 2–10 keV, the fit is not acceptable for either spectrum because of a slight data excess in the $< 2$ keV range.

We accordingly added a Raymond-Smith (R-S) plasma emission component (Raymond, Smith 1977) to the model spectrum, as is often seen in the spectra of spiral galaxies (MA94; SEA95). We left its temperature and normalization free, and assumed that it is absorbed only by the galactic line-of-sight column. We fixed the R-S abundance at 0.4-times solar one (MA94; SEA95), assuming the solar-abundance ratios. Thus, as shown in table 3, the GIS fit has become acceptable, indicating that the soft component is statistically significant. The R-S temperature, 0.6–1.1 keV, is similar to those obtained in other spirals (see subsection 4.6); $\Gamma$ remained nearly unaffected by introducing the soft component. The best-fit models are shown in figure 6 together with the full-range spectra. However, the thermal flux required by the SIS spectrum is much less than that required by the GIS spectrum, and the SIS and GIS values for the column density to the power-law component are inconsistent with each other. Furthermore, the SIS fit is still formally unacceptable. These problems did not vanish, even if we let the overall abundance float.

The above discrepancy could arise if the thermal emission is extended, because the poorer position resolution of the GIS would then reduce the contrast of the nuclear point source relative to the extended emission. To examine this possibility, we again varied the data-integration radius; however, the fit parameters did not significantly change for either instrument. This means that the thermal source is mostly confined to within 3′ (3 kpc) of the nucleus, as for the Fe-K line. Resolving the remaining spectral discrepancy between the two instruments would require a further effort concerning instrumental calibration, which is beyond the scope of the present paper.

### *3.4. Background Emission from the M81 Galaxy*

Our data-integration radii around X-5 are relatively large (1.6 kpc or 3.1 kpc). Therefore, before ascribing the X-5 properties to the M81 nucleus, we must evaluate any possible contamination from "galaxy background", i.e., various non-nuclear X-ray components in M81. Although the soft R-S component may prevail below $\sim$ 2 keV, above 2 keV the largest contribution is expected to come from low-mass X-ray binaries (LMXBs; Fabbiano 1989). The brightest LMXBs have been resolved with Einstein (Elvis, Van Speybroeck 1982; FA88), while fainter ones will make an unresolved extended background (FA88). The Einstein sources X-2, X-3, and X-7 (FA88) fall in the larger of our two integration radii, while X-6 and SN 1993J make partial contributions (subsection 2.3).

We derived a 2–10 keV radial X-ray brightness profile around X-5, by integrating the GIS data from observations 7–9, over a position angle range of $-135°$ to

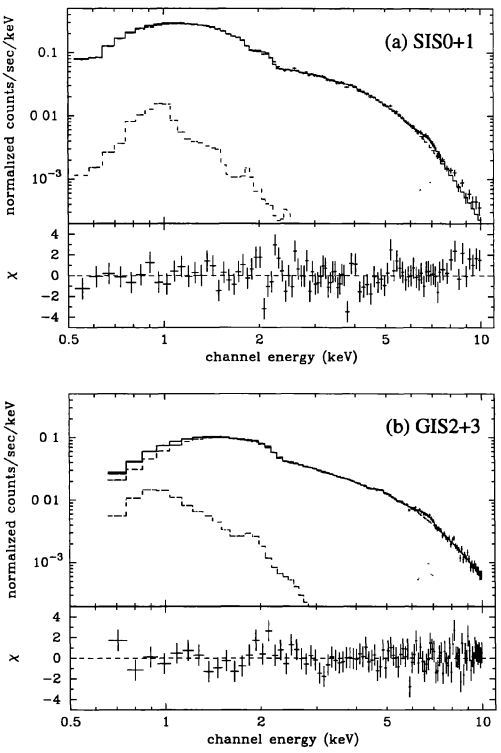


Fig. 6. Same as figure 4, but shown over the full energy bands. The solid lines indicate the best-fit solution of Model 2 in table 3, which consists of three components; a Raymond-Smith model (dot-dashed), an absorbed power-law (dashed), and a broad Gaussian distribution (dotted). The fit is not simultaneous between the two instruments.

45° (to avoid X-6, SN 1993J, and X-9). Its comparison with the point-spread function has revealed an extended emission outside $\sim 3'$, up to at least $10'$. This galaxy background shows a 2–10 keV luminosity of $\sim 2 \times 10^{39}$ erg s$^{-1}$ when integrated over the 180° sector of $3' - 10'$ annulus, and its 0.7–10 keV spectrum can be fitted well with a moderately absorbed ($< 3 \times 10^{21}$ cm$^{-2}$), hot ($> 8$ keV) bremsstrahlung. Comparing these results with those from M31 (Makishima et al. 1989), we can safely ascribe the observed M81 galaxy background to the integrated emission from LMXBs. However, within $\sim 3'$ of the nucleus, the galaxy background brightness is highly uncertain, because the X-5 radial profile becomes indistinguishable from the point-spread function.

To more directly evaluate the LMXB contribution to the X-5 spectra of figure 4, we fitted them using a model consisting of a power-law, a Gaussian distribution, and a LMXB component (a thermal bremsstrahlung with temperature fixed to 10 keV, absorbed with a fixed column of $2 \times 10^{21}$ cm$^{-2}$; Makishima et al. 1989). The SIS and GIS spectra consistently restricted the LMXB contribution to $< 12\%$ (90% confidence) of the 2–10 keV luminosity of X-5. This is consistent with the spill-over flux from X-6 and SN 1993J, as estimated in subsection 2.3. Even allowing the largest possible LMXB contribution, $\Gamma$ steepens only by 0.03. We thus conclude that the ASCA spectra of X-5 are approximately free from the galaxy background.

We also examined the ROSAT HRI image (figure 1b) taken from the archival data, where the nucleus, off-nuclear point sources including SN 1993J, and diffuse or unresolved galaxy emission are seen. The nucleus exhibited a luminosity (Boller et al. 1992) similar to that which we observed. We found that, of the total $\sim 6200$ HRI signal X-rays within $3'$ of the nucleus, at least 82% is confined to within $0'.5$. The galaxy background within $3'$ is thus estimated to be 18% at most in the soft X-ray band; this must partially come from the soft thermal emission, as we observed (figure 6). Therefore, the galaxy background within $3'$ must be even lower in $> 2$ keV, thus providing independent support to the above conclusion.

## 4. Discussion

### *4.1. Identification of X-5 with the Active Nucleus of M81*

We have detected a factor of $\sim 1.7$ X-ray variation from X-5 over a time span of 2 years; also, the observed 2–10 keV flux range is consistent with those recorded from past observations, $(1.4\text{–}2.9) \times 10^{-11}$ erg cm$^{-2}$ s$^{-1}$ (table 3 of PEA93). We also detected $\sim 20\%$ intensity changes on a time scale of one day. These results have established the variability of X-5 much more convincingly than before. This, combined with the clear non-thermal nature of the X-5 spectra above 2 keV (table 2), makes the starburst interpretation of X-5 unlikely.

The variability implies that X-5 consists of a single, or at most a small number of, presumably accretion-powered compact object(s). However, an assembly of ordinary LMXBs cannot provide an explanation, since X-5 is pointlike ($< 70$ pc; Elvis, Van Speybroeck 1982), and the observed X-5 spectra are inconsistent with those of the LMXBs. In addition, the 2–10 keV luminosity of X-5, $\sim 2 \times 10^{40}$ erg s$^{-1}$ on the average, would require $\sim 10^2$ LMXBs emitting at the Eddington limit, so that the variability would be much smaller than was observed. Therefore, as argued by Elvis and Van Speybroeck (1982), X-5 must be either an LLAGN, or a "super-Eddington" X-ray source, which are sometimes found in nearby galaxies (Fabbiano 1989).

The high quality ASCA spectra of X-5 above $\sim 2$ keV are well characterized by a single power-law (plus the iron line), with little contribution from the LMXB-type component. From tables 2 and 3, we quote the photon

index to be $\Gamma = 1.85 \pm 0.04$. (In figure 2, $\Gamma$ is somewhat smaller since the Fe-K line was not separately modeled.) This spectrum is similar to those of Seyfert nuclei, but not with the spectra of super-Eddington sources, which generally resemble those of the LMXBs (MA94; Okada et al. 1994). Considering further the positional coincidence of X-5 with the M81 nucleus (within $\sim 10''$; Elvis, Van Speybroeck 1982), we can confirm the identification of X-5 as an LLAGN made by previous X-ray observations and optical investigations (Filippenko, Sargent 1988; Ho et al. 1996).

### *4.2. Possible Prevalence of LLAGNs*

The M81 nucleus exhibits an H$\alpha$ emission line with a broad component, and its H$\alpha$ to X-ray luminosity ratio is similar to those of Seyfert galaxies (Elvis, Van Speybroeck 1982; Filippenko, Sargent 1988). We therefore infer that the optical lines from M81 are powered by the power-law X-rays from the LLAGN.

Besides M81, LLAGNs have so far been established in a fair number of nearby galaxies (MA94; SEA95), including, e.g., M106 = NGC 4258 (Makishima et al. 1994; Miyoshi et al. 1995), NGC 3642, NGC 4278 (Koratkar et al. 1995), M104 = NGC 4594 (Terashima et al. 1994), NGC 1097 (Iyomoto et al. 1996), and M51 = NGC 5194 (Makishima et al. 1990; MA94; Terashima et al. 1996, in preparation). These galaxies are classified as LINERs and, furthermore, exhibit a weak, but broad, H$\alpha$ component. We therefore suggest that LINERs, particularly those with broad H$\alpha$ components, have a rather high probability to harbor LLAGNs. Since LINERs are rather numerous (Filippenko, Sargent 1985; Ho et al. 1995), this further suggests that a fair fraction of apparently normal galaxies host LLAGNs.

The 2–10 keV luminosities of these LLAGNs, typically $(1\text{–}10) \times 10^{40}$ erg s$^{-1}$, smoothly connect to the lowest end of the Seyfert luminosity function ($10^{41.5-44}$ erg s$^{-1}$). Therefore, the AGN luminosity function may well extend below $\sim 10^{42}$ erg s$^{-1}$ (Mushotzky 1993; Koratkar et al. 1995; SEA95), and the LLAGN contribution to the cosmic X-ray background may not be ignored. Although this inference supports the prediction by Elvis et al. (1984) based on the H$\alpha$ luminosity distributions, it may contradict the results by Persic et al. (1989).

### *4.3. Hard Power-Law Continuum*

The power-law index, $\Gamma = 1.85 \pm 0.04$, that we derived for the M81 nucleus is consistent with those of the type-1 Seyferts (SEA95) as well as that of the M106 nucleus ($\Gamma = 1.78 \pm 0.29$; Makishima et al. 1994), which is another convincing example of LLAGN (Miyoshi et al. 1995). However, our value of $\Gamma$ is significantly smaller (flatter) than those obtained for the M81 nucleus in previous X-ray studies. Even putting aside the very steep index of $\Gamma = 4^{+2}_{-1.5}$ (FA88), obtained with the Einstein IPC (which may be related to the marked faintness of X-5 at that time; see PEA93), observations with EXOSAT, Ginga, BBXRT, and ROSAT consistently yielded $\Gamma = 2.0\text{–}2.2$ with relatively small uncertainties (table 3 of PEA93). The time variability cannot provide a solution to this discrepancy, since during the ASCA observations $\Gamma$ stayed in the 1.7–1.9 range, while the X-ray flux was consistent with those observed previously, except for the Einstein IPC flux (PEA93).

Among these previous results, since the EXOSAT ME (Barr et al. 1985) and Ginga LAC (Ohashi et al. 1992) results were obtained with non-imaging proportional counters, they may be contaminated by other point sources (e.g., X-9; FA88) in the M81 region, and by extended emission components associated with M81. The BBXRT spectrum may have been contaminated similarly, even though the soft thermal component was resolved spectrally by PEA93. On the other hand, the ROSAT PSPC result (Boller et al. 1992), although based on an image, may have been affected by thermal emission from the nuclear region (which we detected), since the value of $\Gamma = 2.0^{+0.16}_{-0.15}$ was derived via a simple single-model fit. Thus, the previously obtained steeper spectra can be explained away in a reasonable way.

We have obtained a relatively small intrinsic absorption ($< 2 \times 10^{21}$ cm$^{-2}$) for the hard component of the M81 nucleus (a factor of 2–4 smaller than was obtained by PEA93). This is in contrast to the case of the M106 nucleus, which is absorbed with $\sim 1.5 \times 10^{23}$ cm$^{-2}$ (Makishima et al. 1994). Considering that the M106 nucleus is certainly seen almost edge-on through the molecular disk (Miyoshi et al. 1995), the difference in absorption between the nuclei of M81 and M106 is most naturally attributed to the difference in the viewing angle with respect to the gaseous disk around the nucleus. This is essentially the same as unification models, which accounts for the difference between type-1 and type-2 Seyfert galaxies (e.g., Antonucci, Miller 1985; Awaki et al. 1991).

These spectral properties cause the LLAGNs look in many respects like scaled-down versions of Seyfert galaxies. However, the trend seen in Seyfert 1/2 galaxies, that the fraction of the obscured objects increases with decreasing intrinsic luminosity (Lawrence, Elvis 1982), does not seem to extend to LLAGNs (Mushotzky 1993). The Compton-reflection effect may be less significant in LLAGNs than in Seyfert galaxies (subsection 3.2; Mushotzky 1993). Furthermore, there are two more X-ray dissimilarities between the M81 nucleus and Seyfert galaxies; Fe-K line energy, and rapid variability (Mushotzky 1993), which we discuss in the following two subsections. These suggest that caution should be exercised before regarding the LLAGNs and Seyfert galaxies as comprising a single and homogeneous class of objects.

### 4.4. *Iron Emission Line*

We have detected an iron-K emission line from the M81 nucleus with an equivalent width of $\sim 170$ eV. Although PEA93 did not detect narrow Fe-K lines from the M81 nucleus with an upper limit equivalent width of 90 eV, their results may be reconciled with ours by the fact that we observed the line to be apparently broad (Gaussian $\sigma \sim 0.2$ keV; figure 5). Evidence of an Fe-K emission line centered at $6.77 \pm 0.45$ keV was obtained in the Ginga spectrum of M81 plus M82; its equivalent width becomes $330 \pm 210$ eV if all of the line photons are assumed to come from M81 (Tsuru 1992). Considering the absence of Fe-K lines in the ASCA spectrum of M82 (Tsuru et al. 1994), this may actually be the case, suggesting consistency between the Ginga and ASCA observations.

The Fe-K lines from AGNs are generally thought to arise via reprocessing of the hard power-law continuum from the nucleus by surrounding material (e.g., the accretion disk; e.g., Pounds et al. 1990; Awaki et al. 1991; Nandra 1991). When the reprocessing material is nearly neutral, we expect a fluorescence Fe-K line to appear at 6.40 keV in the local rest frame (Makishima 1986). When the material is significantly photoionized, so that the dominant ionization states are helium-like or hydrogen-like, the Fe line appears at rest-frame energies of 6.7 or 6.9 keV, respectively.

The iron line profile of the M81 nucleus is reminiscent of the broad and asymmetric Fe-K line profiles observed with ASCA from several Seyfert galaxies (Fabian et al. 1994; Mushotzky et al. 1995; Tanaka et al. 1995), which have been interpreted in terms of gravitational redshift and Doppler effects in the accretion disks seen at an inclination of $\sim 20°$. However, while the iron line flux in these Seyfert galaxies is mostly limited to $< 6.4$ keV in the source rest frame, the present results indicate a considerably higher center energy, $6.65 \pm 0.15$ keV (figure 5). This is one difference between the M81 nucleus and the AGN.

This difference in the line-center energy may be explained in several ways (SEA95). First, the M81 line photons may be a blend of separate narrow lines: e.g., a 6.4 keV line and a 6.7 keV line. In fact, the GIS line feature can also be modeled by two narrow lines at $\sim 6.3$ and $\sim 6.8$ keV, although the SIS data somewhat prefer a single broad line. Second, since it is possible that the accretion disk has a higher inclination than those in Seyfert-1 galaxies ($\sim 20°$), the blue-shifted component due to the longitudinal Doppler effect is enhanced. Indeed, in the type-2 Seyfert galaxy IRAS 18325−5926, a broad iron line has been observed at 6.8–6.9 keV in the source rest frame (Iwasawa et al. 1995). A third possibility is that the line-producing region in the M81 nucleus is significantly more photoionized than in those of Seyfert galaxies. Further discussion concerning the Fe-K line will be presented in a forthcoming paper (Yaqoob et al. 1996, in preparation).

### 4.5. *Time Variation*

Some Seyfert galaxies (particularly of low-luminosity ones) exhibit pronounced intensity variations on time scales as short as $10^{3-4}$ s, by more than a factor of a few (e.g., Lawrence et al. 1987; McHardy, Czerny 1987; Kunieda et al. 1992; Krolik et al. 1993). In contrast, variations of the M81 nucleus on these time scales were much less conspicuous; even on longer time scales, its variation (figure 2a) is considerably smaller than those of Seyfert galaxies. Filippenko, Sargent (1988) and Ho et al. (1996) report that the H$\alpha$ emission from the M81 nucleus is stable, unlike in Seyfert galaxies. No rapid X-ray variability was detected from the LLAGNs in M106 (Makishima et al. 1994) or in NGC 1097 (Iyomoto et al. 1996), either. These pieces of evidence illustrate another potential difference between LLAGNs and Seyferts (Mushotzky et al. 1993)

The power-density spectrum (PDS) $P(\nu)$ of the intensity variation in Seyfert galaxies and Galactic black-hole candidates can be modeled as

$$P(\nu) = \begin{cases} P_0 & (\nu < \nu_{\rm k}) \\ P_0\,(\nu/\nu_{\rm k})^{-\alpha} & (\nu > \nu_{\rm k}) \end{cases}, \qquad (1)$$

where $P_0$, $\alpha$, and $\nu_{\rm k}$ (knee frequency) are constants. Seyfert galaxies typically exhibit $\alpha = 1$–2 (Lawrence et al. 1987; McHardy, Czerny 1987; Hayashida et al. 1995), and Hayashida et al. (1995) derived $\nu_{\rm k} \sim 5 \times 10^{-5}$ Hz for NGC 4051 and MCG−6–30–15. From Galactic black-hole candidates, we typically observe $\alpha \sim 1.4$ and $\nu_{\rm k} \sim 0.1$ Hz (e.g., Makishima 1988).

Suppose that we repeatedly observe an X-ray source whose PDS is represented by equation (1), determine the intensity over an integration time of $T_1$ each, and obtain a light curve of the total time span $T_2$ when $T_1 \ll T_2$. Then, even for a fairly uneven data sampling, the root-mean-square fractional variation $V$ of the light curve may be approximated as

$$V(T_1, T_2)^2 = c \int_{\nu_2}^{\nu_1} P(\nu)\, d\nu, \qquad (2)$$

where $\nu_i = T_i^{-1}$ $(i = 1, 2)$, and $c$ is an appropriate constant. In the present case, the long-term light curve (figure 2) gives $T_1 = 3 \times 10^4$ s (typical duration of each observation; table 1) and $T_2 = 6 \times 10^7$ s (2 years) together with $V(T_1, T_2) = 0.22$, while the short-term light curve (figure 3) implies $T_1 = 600$ s, $T_2 = 2 \times 10^4$ s, and $V(T_1, T_2) = 0.08$. By substituting these results into equation (2), and utilizing equation (1) with $\alpha = 1.5$, we can eliminate the normalization product $P_0\, c$. We have thus obtained for the M81 nucleus $\nu_{\rm k} = (1\text{–}3) \times 10^{-6}$ Hz. This knee frequency is significantly lower than those of the rapidly varying Seyferts, and seems to be closer to that of some quasars (Hayashida et al. 1995).

Although the physical mechanism accounting for equation (1) is not understood, a lower value of $\nu_k$ is thought to indicate a longer scale length, hence a larger black-hole mass (e.g., Wandel, Mushotzky 1986; Hayashida et al. 1995). We therefore suggest that the mass of the M81 nucleus, and of other LLAGNs in general, is larger than those of the fast-varying Seyfert nuclei, and that their very low luminosities are a result of extremely small accretion rates (Iyomoto et al. 1996). Actually, M106 has a nuclear mass of $3.6\times10^7\ M_\odot$ (Miyoshi et al. 1995) and an accretion rate as small as $\sim 7\times10^{-6}$ times the Eddington accretion rate (derived from the ASCA luminosity of Makishima et al. 1994). However, we cannot yet exclude the possibility that the reduced variability in LLAGNs is a direct consequence of the very low accretion rate itself, rather than being due to the large central mass. The X-ray variation is also insignificant in some type-2 Seyfert galaxies (e.g., NGC 1068; Ueno et al. 1994), presumably due to the predominance of reprocessed X-ray components. However, this cannot be the case in the M81 nucleus, since it lacks reprocessing signatures, such as absorption edges, very flat X-ray continua ($\Gamma \sim 1.3$; Ueno et al. 1994), Compton reflection components (subsection 3.2), or *neutral* fluorescence lines (Fukazawa et al. 1994).

### *4.6. Soft Thermal Emission*

Within 3 kpc of the M81 nucleus, we have detected thermal emission with a sub-keV temperature and a 0.5–3 keV luminosity of $(0.4\text{–}1.5)\times10^{39}$ erg s$^{-1}$. If we assume that the extended (or unresolved) X-ray emission seen in the ROSAT HRI map (subsection 3.4) has a similar thermal spectrum, its 0.5–3 keV luminosity in an annular region of radius 0.′5–3′ from the nucleus is estimated to be $\sim 1\times10^{39}$ erg s$^{-1}$, which agrees with the ASCA results. On the other hand, although PEA93 obtained evidence for a similar thermal component using BBXRT, their thermal flux is 5–20 times larger than ours. Presumably, as a result of the larger aperture, the BBXRT spectrum included a significant contribution from a much larger part of the M81 galaxy.

From a number of spiral galaxies, ASCA has detected similar soft thermal X-ray components which have typical temperatures of 0.5–1.0 keV and often sub-solar abundances (MA94; Terashima et al. 1994; SEA95; Iyomoto et al. 1996). The 0.5–4 keV luminosities of such components vary from galaxy to galaxy over the range $10^{38-40}$ erg s$^{-1}$ (SEA95). These components may well come from heterogeneous origins, including supernova remnants, hot plasmas associated with jets (e.g., in M106; Makishima et al. 1994), thermal gas created in the nuclear starburst region (e.g., in M82; Tsuru et al. 1994), and reprocessing of the hard nuclear X-rays by photoionized material. Thus, the nature of the M81 thermal component is yet to be investigated.

## 5. Summary and Conclusion

Through a series of observations of the M81 region with ASCA, we have shown that its nucleus can be regarded as an LLAGN (low-luminosity AGN). We observed both long-term and short-term intensity variations. The characteristic time scale of the variation of the M81 nucleus is inferred to be $\sim$ 10 days, which may be longer than those of Seyfert galaxies, but similar to those of quasars. We speculate that some LLAGNs, if not all, have larger central masses than those of Seyfert galaxies.

The spectrum of the M81 nucleus consists of a hard power-law continuum, an iron-K line, and a soft thermal component. The power-law index was found to be stable at $\Gamma \sim 1.85$, with relatively low intrinsic absorption ($\sim 1\times10^{21}$ cm$^{-2}$). Therefore, the M81 nucleus can be regarded as being a typical LLAGN without heavy obscuration, in contrast to the strongly absorbed M106 nucleus. The nature of the thermal component is yet to be specified.

The observed iron line is broad ($\sigma \sim 0.2$ keV), or complex, and exhibits an equivalent width of $170 \pm 60$ eV. When compared to the Fe-K lines observed from Seyfert galaxies, the Fe-K line of the M81 nucleus has a similar profile, but a significantly higher line center energy ($\sim$ 6.65 keV). This difference allows for several alternative explanations.

We thank all of the members of the ASCA team for the mission management, including spacecraft operation, data acquisition, and instrumental calibration. We thank Tahir Yaqoob and Andy Ptak for helpful discussions and comments.

## References

Antonucci R.R.J., Miller J.S. 1985, ApJ 297, 621
Awaki H., Koyama K., Inoue H., Halpern J. 1991, PASJ 43, 195
Barr P., Giommi P., Wamsteker W., Gilmozzi R., Mushotzky R. 1985, BAAS 17, 608
Bartel N., Shapiro I.I., Corey B.E., Marcaide J.M., Rogers A.E.E., Whitney A.R., Cappallo R.J., Graham D.A. 1982, ApJ 262, 556
Beck R., Klein U., Krause M. 1985, A&A 152, 237
Boller Th., Meurs E.J.A., Brinkmann W., Fink H., Zimmermann U., Adorf H.-M. 1992, A&A 261, 57
Burke B.E., Mountain R.W., Daniels P.J., Dolat V.S. 1994, IEEE Trans. Nuc. Sci. 41, 375
Burke B.E., Mountain R.W., Harrison D.C., Bautz M.W., Doty J.P., Ricker G.R., Daniels J.P. 1991, IEEE Trans. ED-38, 1069
Elvis M., Soltan A., Keel W.C. 1984, ApJ 283, 479
Elvis M., Van Speybroeck L. 1982, ApJL 257, L51
Fabbiano G. 1988, ApJ 325, 544 (FA88)

Fabbiano G. 1989, ARA&A 27, 87
Fabian A.C., Kunieda H., Inoue S., Matsuoka M., Mihara T., Miyamoto S., Otani C., Ricker G. et al. 1994, PASJ 46, L59
Filippenko A.V., Sargent W.L.W. 1985, ApJS 57, 503
Filippenko A.V., Sargent W.L.W. 1988, ApJ 324, 134
Freedman W.L., Hughes S.M., Madore B.F., Mould J.R., Lee M.G., Stetson P., Kennicutt R.C., Turner A. et al. 1994, ApJ 427, 628
Fukazawa Y., Makishima K., Ebisawa K., Fabian A.C., Gendreau K.C., Ikebe Y., Iwasawa K., Kii T. et al. 1994, PASJ 46, L141
Garcia F. 1993, IAU Circ. No.5731
Hayashida K. et al. 1995, ApJ submitted
Ho L.C., Filippenko A.V., Sargent W.L.W. 1995, ApJS 98, 477
Ho L.C., Filippenko A.V., Sargent W.L.W. 1996, ApJ in press
Ishisaki Y. 1994, in New Horizon of X-Ray Astronomy, ed F. Makino, T. Ohashi (Universal Academy Press, Tokyo) p505
Iwasawa K. et al. 1995, MNRAS submitted
Iyomoto N., Makishima K., Fukazawa Y., Tashiro M., Ishisaki Y., Nakai N., Taniguchi Y. 1996, PASJ 48, 231
Kohmura Y. 1994, PhD Thesis, The University of Tokyo
Kohmura Y., Fukazawa Y., Ikebe Y., Ishisaki Y., Kamijo Y., Kaneda Y., Makishima K., Matsushita K. et al. 1993, Proc. SPIE 2006, 79
Kohmura Y., Inoue H., Aoki T., Ishida M., Itoh M., Kotani T., Tanaka Y., Ishisaki Y. et al. 1994, PASJ 46, L157
Koratkar A., Deustua S.E., Heckman T., Filippenko A.V., Ho L.C., Rao M. 1995, ApJ 440, 132
Krolik J., Done C., Madejski G. 1993, ApJ 402, 432
Kunieda H., Hayakawa S., Tawara Y., Koyama K., Tsuruta S., Leighly K. 1992, ApJ 384, 482
Kwan J., Krolik J. 1981, ApJ 250, 478
Lawrence A., Elvis M. 1982, ApJ 256, 410
Lawrence A., Watson M., Pounds K.A., Elvis M. 1987, Nature 325, 694
Makishima K. 1986, in Physics of Accretion onto Compact Objects, ed K.O. Mason, M.G. Watson, N.E. White (Springer-Verlag, Berlin) p249
Makishima K. 1988, in Physics of Neutron Stars and Black Holes, ed Y. Tanaka (Universal Academy Press, Tokyo) p175
Makishima K. 1994, in New Horizon of X-Ray Astronomy, ed F. Makino, T. Ohashi (Universal Academy Press, Tokyo) p171 (MA94)
Makishima K., Fujimoto R., Ishisaki Y., Kii T., Loewenstein M., Mushotzky R., Serlemitsos P., Sonobe T. et al. 1994, PASJ 46, L77
Makishima K., Ohashi T., Hayashida K., Inoue H., Koyama K. 1989, PASJ 41, 697
Makishima K., Ohashi T., Kondo H., Palumbo G.G.C., Trinchieri G. 1990, ApJ 365, 159
Makishima K., Tashiro M., Ebisawa K., Ezawa H., Fukazawa Y., Gunji S., Hirayama M., Idesawa E. et al. 1996, PASJ 48, 171
McHardy I., Czarny B. 1987, Nature 325, 696
Miyoshi M., Moran J., Herrnstein J., Greenhill L., Nakai N., Diamond P., Inoue M. 1995, Nature 373, 127
Mushotzky R.F. 1993, in The Nearest Active Galaxies, ed J. Beckman, L. Colina, H. Netzer (Consejo Superior de Investigaciones Cientificicas Madrid) p47
Mushotzky R.F., Fabian A.C., Iwasaka K., Kunieda H., Matsuoka M., Nandra K., Tanaka Y. 1995, MNRAS 272, L9
Nandra K. 1991, PhD Thesis, Leicester University
Ohashi T., Ebisawa K., Fukazawa Y., Hiyoshi K., Horii M., Ikebe Y., Ikeda H., Inoue H. et al. 1996, PASJ 48, 157
Ohashi T., Makishima K., Mihara T., Tsuru T., Awaki H., Koyama K., Takano S., Kondo H. 1992, in Windows on Galaxies, ed G. Fabbiano et al. (Kluwer Academic Press, Dordrecht) p243
Okada K., Mihara T., Makishima K. 1994, in New Horizon of X-Ray Astronomy, ed F. Makino, T. Ohashi (Universal Academy Press, Tokyo) p515
Peimbert M., Torres-Peimbert S. 1981, ApJ 245, 845
Persic M., De Zotti G., Danese L., Palumbo G.G.C., Franceschini A., Boldt E.A., Marshall F.E. 1989, ApJ 344, 124
Petre R., Mushotzky R.F., Serlemitsos P.J., Jahoda K., Marshall F.E. 1993, ApJ 418, 644 (PEA93)
Pounds K.A., Nandra K., Stewart G.C., George I.M., Fabian A.C. 1990, Nature 344, 132
Raymond J.C., Smith B.W. 1977, ApJS 35, 419
Serlemitsos P.J., Jalota L., Soong Y., Kunieda H., Tawara Y., Tsusaka Y., Suzuki H., Sakima Y. et al. 1995a, PASJ 47, 105
Serlemitsos P.J., Ptak A., Yaqoob T. 1995b, in The Physics of LINERS (Space Science Telescope Institute, Baltimore) (SEA95)
Shuder J.M., Osterbrock D.E. 1981, ApJ 250, 55
Tanaka Y., Inoue H., Hold S.S. 1994, PASJ 46, L37
Tanaka Y., Nandra K., Fabian A.C., Dotani T., Hayashida K., Iwasawa K., Kii T., Kunieda H. et al. 1995, Nature 375, 659
Terashima Y., Serlemitsos P.J., Kunied H., Iwasawa K. 1994, in New Horizon of X-Ray Astronomy, ed F. Makino, T. Ohashi (Universal Academy Press, Tokyo) p523
Terlevich R., Melnick J. 1985, MNRAS 213, 841
Tsuru T. 1992, PhD Thesis, The University of Tokyo
Tsuru T., Hayashi I., Awaki H., Koyama K., Fukazawa Y., Ishisaki Y., Iwasawa K., Ohashi T. et al. 1994, in New Horizon of X-Ray Astronomy, ed F. Makino, T. Ohashi (Universal Academy Press, Tokyo) p529
Tsusaka Y., Suzuki H., Yamashita K., Kunieda H., Tawara Y., Ogasaka Y., Uchibori Y., Honda H. et al. 1995, Appl. Opt. 34, 4848
Turner T.J., Pounds K.A. 1989, MNRAS 240, 833
Ueno S., Mushotzky R.F., Koyama K., Iwasawa K., Awaki H., Hayashi I. 1994, PASJ 46, L71
Wandel A., Mushotzky R.F. 1986, ApJL 306, L61